Journal of ELECTRONIC MATERIALS, Vol. 46, No. 7, 2017
DOI: 10.1007/s11664-017-5370-7

Highly Sensitive Flexible Human Motion Sensor Based on $ZnSnO_3$/PVDF Composite

YOUNG JIN YANG,[1] SHAHID AZIZ,[1] SYED MURTUZA MEHDI,[2] MEMOON SAJID,[1] SRIKANTH JAGADEESAN,[1] and KYUNG HYUN CHOI[1,3]

1.—Department of Mechatronics Engineering, Jeju National University, Jeju, Korea. 2.—Department of Mechanical Engineering, Nadirshaw Eduljee Dinshaw (NED) University of Engineering and Technology, Karachi, Pakistan. 3.—e-mail: amm@jejunu.ac.kr

A highly sensitive body motion sensor has been fabricated based on a composite active layer of zinc stannate ($ZnSnO_3$) nano-cubes and poly(vinylidene fluoride) (PVDF) polymer. The thin film-based active layer was deposited on polyethylene terephthalate flexible substrate through D-bar coating technique. Electrical and morphological characterizations of the films and sensors were carried out to discover the physical characteristics and the output response of the devices. The synergistic effect between piezoelectric $ZnSnO_3$ nanocubes and β phase PVDF provides the composite with a desirable electrical conductivity, remarkable bend sensitivity, and excellent stability, ideal for the fabrication of a motion sensor. The recorded resistance of the sensor towards the bending angles of $-150°$ to $0°$ to $150°$ changed from 20 MΩ to 55 MΩ to 100 MΩ, respectively, showing the composite to be a very good candidate for motion sensing applications.

Key words: Motion sensor, composite, piezoelectric, PVDF, $ZnSnO_3$

INTRODUCTION

With an increasing amount of research being carried out in the field of artificial skin for advanced robotics, flex and strain sensors are among the major components being studied for this purpose. Other applications of flex sensors include gesture controlled human machine interface devices,[1–5] interpretation of sign language by mounting them on glove fingers,[6–8] health monitoring devices to measure the muscle joint angle and muscle-induced movement,[9–11] and so on. Flex sensors are a simpler form of strain sensors that are only able to detect bending when compared to strain sensors that can also measure elongation or strain. This simplicity, though, limits their operation and application scope, yet makes the flex sensors easier and cheaper to fabricate compared to strain sensors.[2] The working principle of most common and cheap flex sensors is usually based on the change in resistance of the device upon bending at different angles relative to its straight position.[12] Another famous type of flex sensors include fiber optics-based sensors that detect the bending as a function of change in their refractive index and power output.[13] Two-dimensional stress and flex sensors based on metal–oxide–semiconductor field-effect transistors have also been fabricated with a very low detection range and percentage sensitivity and high error.[14]

Resistive sensors, however, are the main focus of current research owing to their low cost and ease of fabrication and use. With the advancement in materials sciences, a wide variety of other materials ranging from carbon nanotubes (CNTs), nanowires, nanoparticles, conductive polymers, graphite along with its derivatives, and composites of some conductive polymers with piezoresistive materials have been studied for their contribution to specific applications in strain sensing.[15–18] Conductive polymer composites show a great potential in piezoresistive

Young Jin Yang and Shahid Aziz can be considered as the first contributing authors for this manuscript.
(Received June 21, 2016; accepted February 10, 2017; published online February 22, 2017)

devices.[19–22] Graphene, graphene oxide, its derivatives, and conductive polymers have been deployed to fabricate resistive strain sensors with good sensitivity, but their mechanical durability and stability are not ideal.[23–26] Single-walled and multi-walled CNTs have also been used for piezoresistive strain sensors due to their unique electromechanical properties.[26–31] Strain sensors based on piezoelectric $ZnSnO_3$ nano-/microwires and their composites with ZnO, CNTs, and other piezoelectric non-polymeric materials have been fabricated, but their durability and sensitivity is not ideal for real-life applications.[32] Similarly, sensors based on piezoelectric polymeric materials like PVDF and its composites with ZnO nanowires have been fabricated with an improved performance.[19,33]

In this work, a composite of zinc stannate ($ZnSnO_3$) and poly(vinylidene fluoride) (PVDF) has been used as the active layer on polyethylene terephthalate (PET) substrate for flex sensing in both positive and negative bending directions. Although $ZnSnO_3$ has excellent piezoelectric properties but its thin film structure is not very robust for sustaining high deformation through bending in both directions. To counter this issue, the PVDF polymer has been introduced to help bind the $ZnSnO_3$ nanocubes together, while maintaining the piezoelectric properties of the film. The effects of the sensor dimensions and the film thickness on their performance has also been investigated. The sensors exhibit excellent responses towards bending angles between −150° and 150° with almost 40% reduction in 0° intrinsic resistance at −150° bend, and a 60% increase at a bend of 150°. A detailed comparison of a wide range of strain and flex sensors based on materials, working principles, sensitivity, stability, and durability has been provided in supplementary information Table 1.

EXPERIMENTAL

Material Synthesis

The cubic crystals of zinc stannate ($ZnSnO_3$) were synthesized through a hydrothermal process[34] from zinc sulfate heptahydrate ($ZnSO_4{\cdot}7H_2O$) and sodium stannate trihydrate ($Na_2SnO_3{\cdot}3H_2O$) precursors. Both the precursors were purchased from Duksan Pure Chemicals, South Korea. The formation of $ZnSnO_3$ nanocubes was confirmed by x-ray diffraction (XRD) spectroscopy, field-emission surface electron microscopy (FE-SEM), Fourier transform infrared (FTIR) spectroscopy, and Raman spectroscopy.[34] PVDF powder, average Mw ~ 534,000, was purchased from Sigma. The solvent [N,N-Dimethylformamide, $HCON(CH_3)_2$, purity ≥ 99.5%] (DMF) was purchased from Daejung Chemicals, Korea, and acetone [CH_3COCH_3] was purchased from Kanto Chemicals, Tokyo, Japan.

PVDF is a semi-crystalline non-centrosymmetric polymer which exhibits piezo-, pyro- and ferroelectric properties. It is a linear polymer that exhibits permanent electric dipoles perpendicular to the direction of the molecular chain. These dipoles are the result of the difference in electronegativity between the atoms of hydrogen and fluorine with respect to carbon. Depending on the processing conditions, PVDF exhibits several different crystalline phases that include α, β, γ, and δ phases. The β phase of PVDF is exhibits the best piezoelectric properties.[19] The structure of the α and β phases of PVDF are shown in Fig. 1 along with the crystal structure of $ZnSnO_3$ nano-cubes.

Ink Preparation

Liquid inks were necessary for the fabrication of sensors owing to the implementation of all printing methods in this research work. The ink for the active layer was formulated by first preparing a 15 wt/vol.% PVDF solution in 20 mL of 1:1 DMF and Acetone solvents. The solution was kept on magnetic stirrer at 1200 rpm for 4 h at 50°C. After the formation of a homogenous solution of PVDF, 4 wt/vol.% $ZnSnO_3$ nanocubes were added into the solution that was again magnetically stirred overnight at room temperature. In order to get a fine and homogenous dispersion of $ZnSnO_3$ nanocubes in the solution, the solution was probe sonicated for 20 min with parameters of 5 s pulse-on, and 2 s pulse-off. The composite ink was ready to be employed in device fabrication at this stage.

Sensor Fabrication

The active layer of the sensors was fabricated using the D-bar coating technique that is a simple, cost-effective, and scalable method for thin-film fabrication. The D-bar coating system and its components are presented in Fig. 2.

Before starting the deposition of the active layer, the PET substrates were first cleaned and then UV-treated for 10 min as a hydrophilic treatment of PET to facilitate the deposition of the $ZnSnO_3$/PVDF active layer. The system photograph presented in Fig. 2 shows a steel rod that rolls over the substrate surface for the fabrication of thin films. The roller does not touch the substrate directly but there is a gap of the order of a few microns between the roller and substrate. The thickness of the deposited film is controlled by adjusting this gap. A larger gap means a higher film thickness and vice versa. After the substrate is placed in position on the printing bed, the rod is moved to the desired height through manual adjustment of the pneumatic control knobs. Once the desired bar height is set, ink is supplied that covers the rod surface which is then slowly rolled on the substrate for thin film deposition. After the deposition of the active layers, the samples were dried at 60°C overnight in furnace. Smaller sensing devices of desired sizes and shapes were later cut off from the main sample. Copper tape was used as electrical contacts for response measurement. The step-by-step

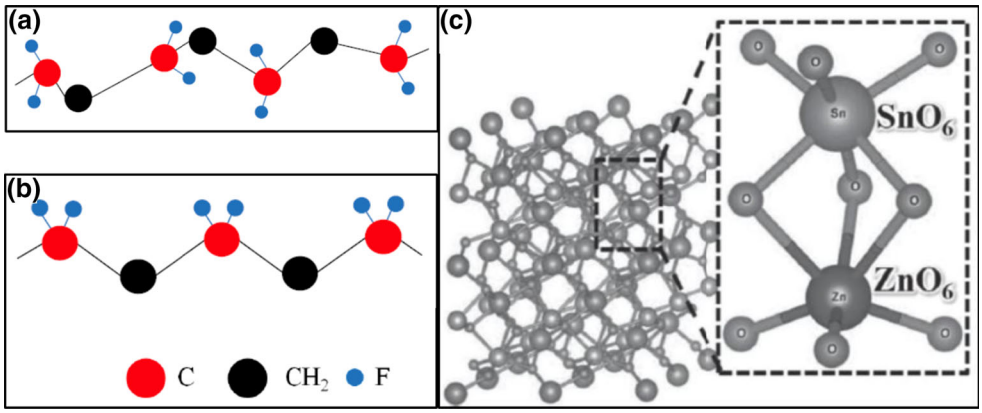

Fig. 1. Structural formulae of PVDF showing (a) α phase, (b) β phase, and (c) crystal structure of $ZnSnO_3$ nanocubes.

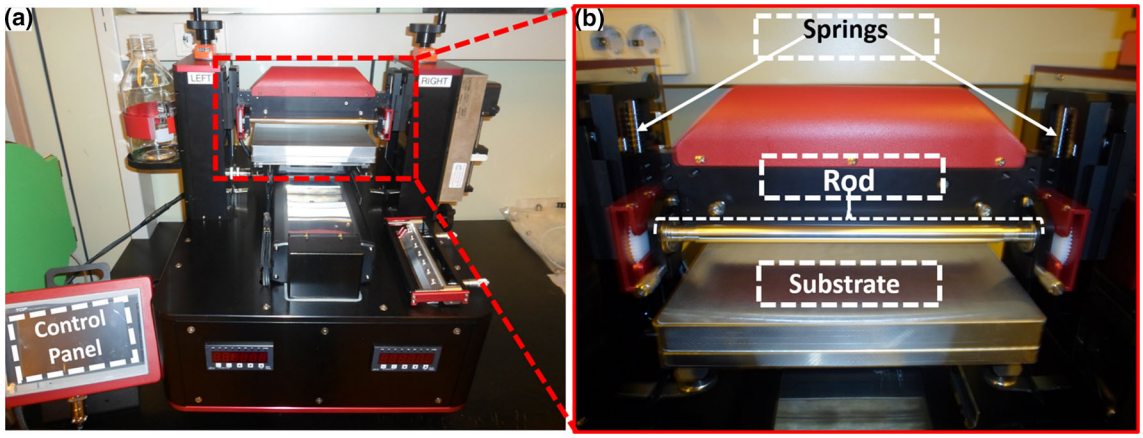

Fig. 2. (a) The semi-automatic D-bar coating system with (b) inset showing the substrate, steel bar in the fixture, and springs for pressure control.

fabrication process and the final device images are presented in Fig. 3.

Sensor Characterizations

The physical, morphological, and electrical characterizations of the sensors were performed to evaluate the performance and attributes of the devices. Optical microscopy was performed at different magnifications using an Olympus BX51M colored microscope. The surface morphology and film thickness of the films was investigated using Jeol JSM-7600F field emission scanning electron microscope. 2D and 3D surface profiles of the films were obtained using a NanoView high accuracy non-contact surface profiler. The electrical response of the sensors was measured using an Applent AT825 digital LCR meter that was connected to a computer through a USB interface for data logging, plotting, and processing. The schematic diagram of the electrical response measurement setup is presented in Fig. 4.

RESULTS AND DISCUSSION

Optical microscopic images of the composite based films are presented in Fig. 5 showing the deposition quality over large areas. The results confirm the deposition of high-quality films with no visible cracks or deformities. They also indicate that the surface roughness of the films is expected to be very high due to the formation of a high-viscosity suspension of $ZnSnO_3$ in PVDF solution.

To measure the surface roughness and confirm the predicted film morphology from optical microscopy, 2D and 3D surface profiles of the films were measured and the results are presented in Fig. 6 and show that the average roughness of the films is 1.4 μm while the maximum z-axis roughness can reach up to 16.8 μm which ascertains the prediction made on film roughness through the microscopic images. High surface roughness provides high physical mobility to the films enabling the operation of sensors for a wide range of bending angles, i.e. $-150°$ to $0°$ to $150°$.

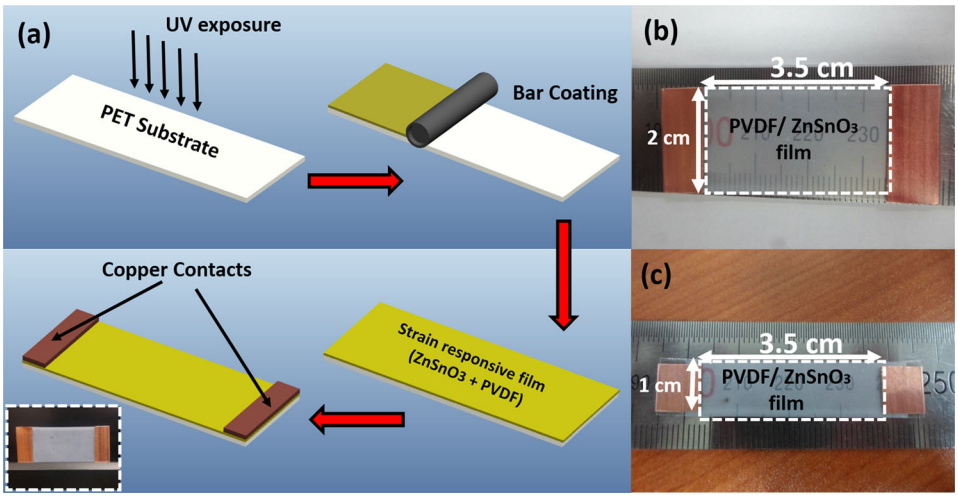

Fig. 3. (a) Schematic illustration of the sensor fabrication process with inset showing the actual sensors having dimensions of (b) 3.5 cm × 2 cm, and (c) 3.5 cm × 1 cm.

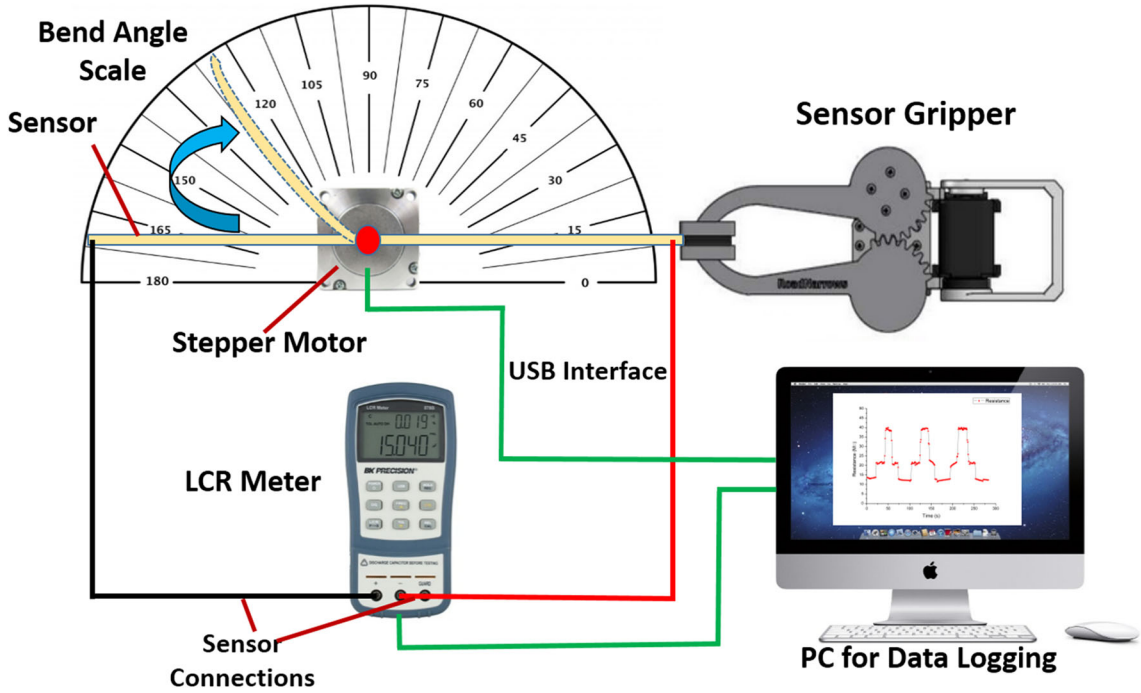

Fig. 4. Schematic diagram of the setup used for measuring the resistive response of the sensors against different bending angles.

Scanning electron microscopy of the films with different thicknesses was performed and the results are presented in Fig. 7. Both surface morphology and film thickness can be observed through the surface SEM and cross-sectional SEM, respectively.

The low-resolution surface profile presented in Fig. 7a clearly indicates the presence of $ZnSnO_3$ nanocubes embedded inside the polymer PVDF matrix. The high-resolution surface image presented in Fig. 7b shows micropores and loosely arranged particles in the film displaying room for their mechanical movement upon the application of external force through bending. This enables the films to have a piezo-resistive effect that can be used for flex sensing applications. The application of force in the inward direction improves the connection between the particles, thus reducing the film resistance and vice versa. The cross-sectional SEM images presented in Fig. 7b and d for the two different samples indicate the thickness of the active layers to be ~2 μm and ~1 μm. The physical morphology of the films was not much affected by changing the film thickness. The effect of thickness on the electrical response of the sensors are presented in Fig. 8a and b. The results show that both sensors show excellent responses upon bending and

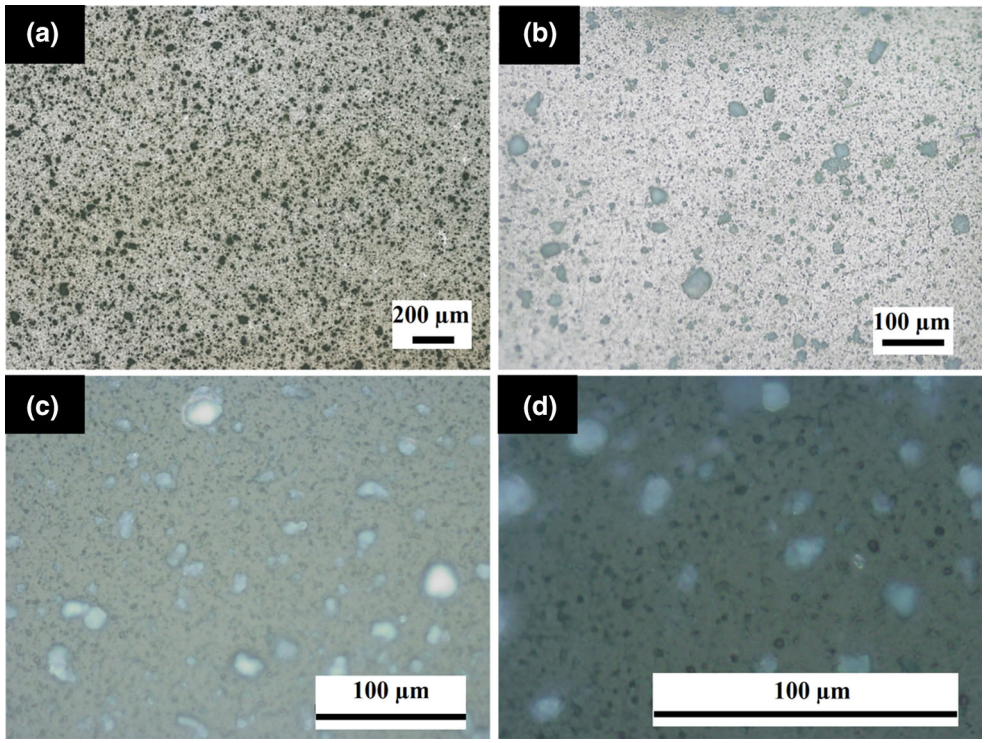

Fig. 5. Microscopic images of the PET substrate coated with $ZnSnO_3$/PVDF composite film at different magnifications of (a) ×5, (b) ×20, (c) ×50, and (d) ×100.

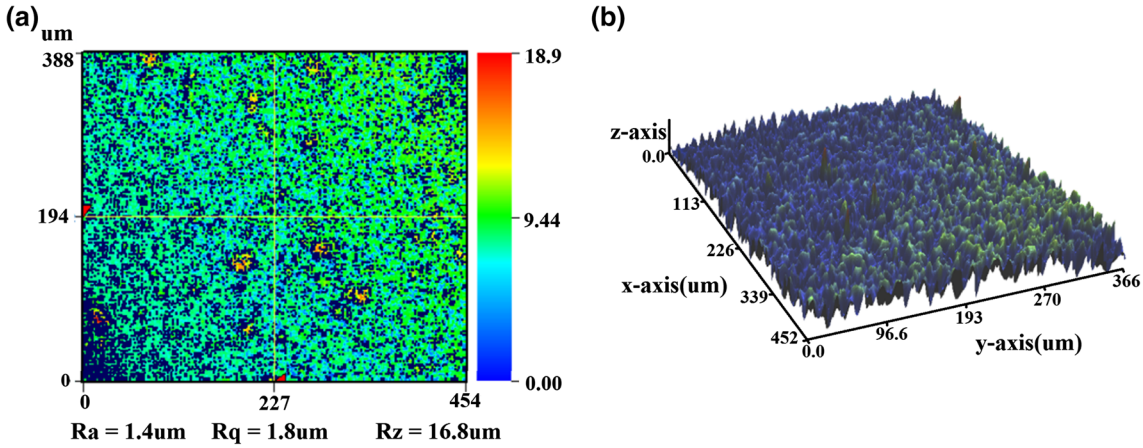

Fig. 6. (a) 2D and (b) 3D surface profiles of the $ZnSnO_3$/PVDF composite film.

that their resistance changes with changing the bending angle. The intrinsic resistance of the sensors with lower film thickness is higher than that of the thick film sensor as expected.

After determining the effect of film thickness, the effect of sensor dimensions was investigated by fabricating two different sensors of varying dimensions. The resistance of the fabricated sensors depends upon the physical properties like length, width, and bend angle, etc. The change in resistance of the different sensors was measured against the bending angles for both the sensors with varying dimensions, and the results are presented in Fig. 9.

It can determined from Fig. 9a that the intrinsic resistance of the sensor with dimensions 3.5 cm × 2 cm is in range of 10s of MΩ's and switches stably between ~13 MΩ to ~40 MΩ for −150° to 150° bend angles. The intrinsic resistance of the sensor with dimensions of 3.5 cm × 1 cm is around twice in magnitude compared with that of the wider sample and switches between ~20 MΩ to ~100 MΩ for −150° to 150° bend angles, as

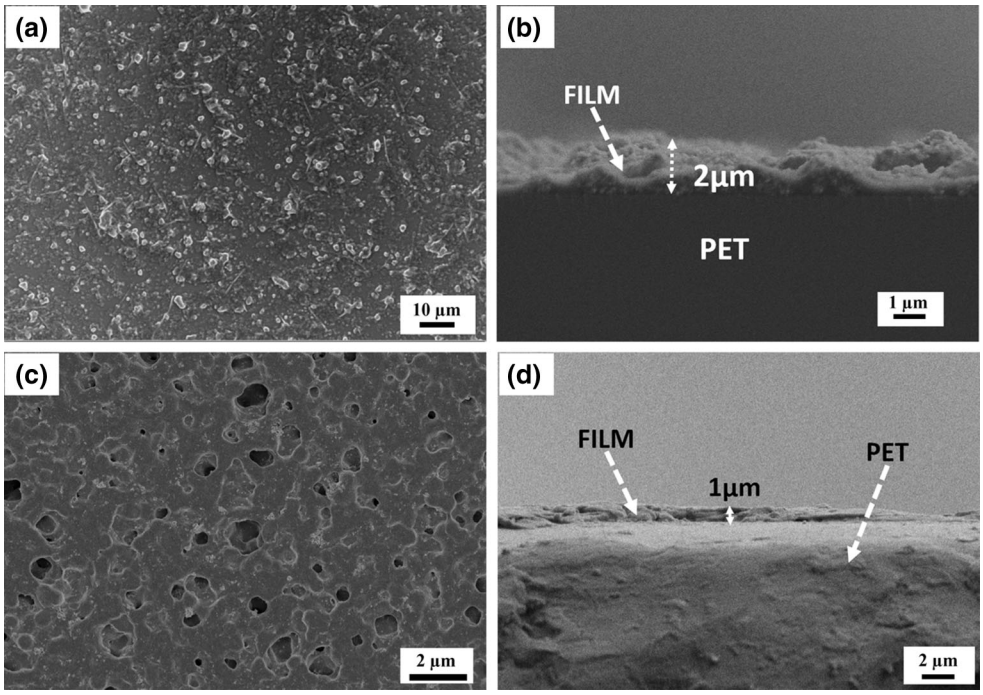

Fig. 7. SEM images of the fabricated films showing (a) surface profile at low magnification, (b) cross-section of sample 1, (c) surface profile at high magnification, and (d) cross-section of sample 2.

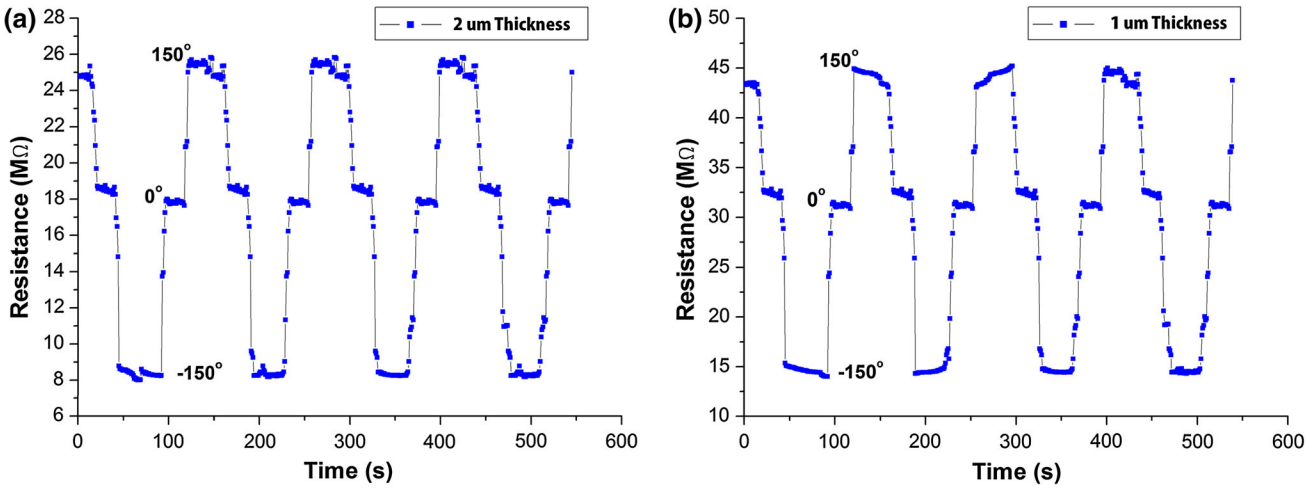

Fig. 8. Resistive response of the sensors with film thickness of (a) 2 μm and (b) 1 μm.

presented in Fig. 9b. This behavior clearly shows the effect of width on the sensor's resistance. The smaller the width, the lower the overall resistance of the sensor, and the factor of change is almost proportional to the ratio of the sensor widths. The sensors were then tested for their durability by recording their resistive response after flexing and bending them for multiple numbers of cycles. The results of the durability test with the sensor response curves after bending for 0 cycles, 500 cycles, and 1000 cycles are presented in Fig. 10. The results show that the sensors show very stable resistive response even after bending for up to 1000 cycles.

This indicates the high robustness of the sensors and prove their worth to be deployed in real-life applications. This highly stable behavior of the sensors is mainly due to the presence of the PVDF polymer that acts as a binding matrix for zinc stannate and prevents cracking and other permanent mechanical deformations in the active layer.

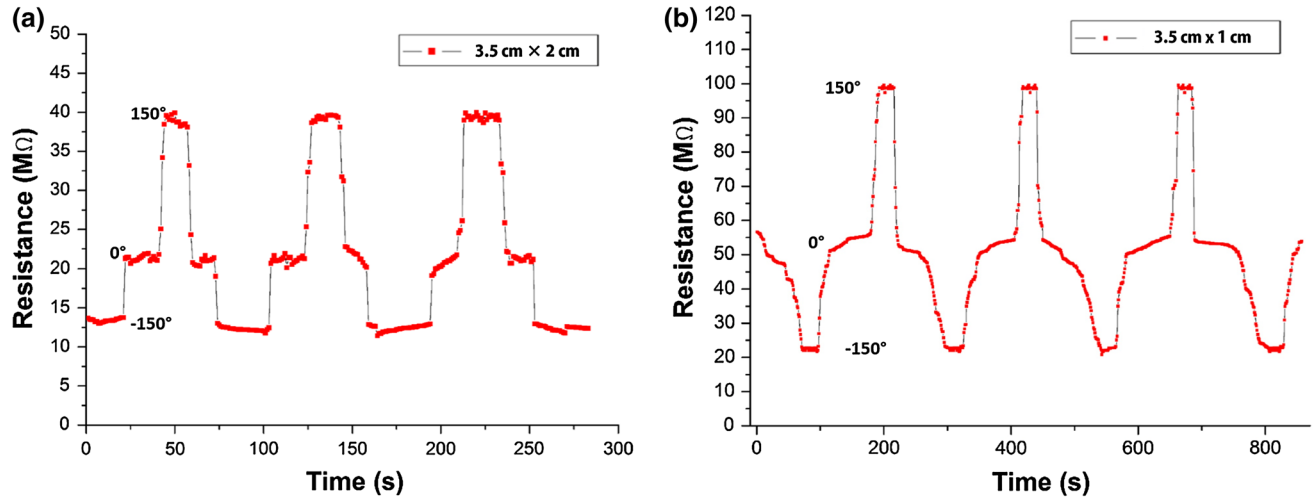

Fig. 9. Response of the sensor for bending angles of −150° to 0° to 150° with dimensions of (a) 3.5 cm × 2 cm and (b) 3.5 cm × 1 cm.

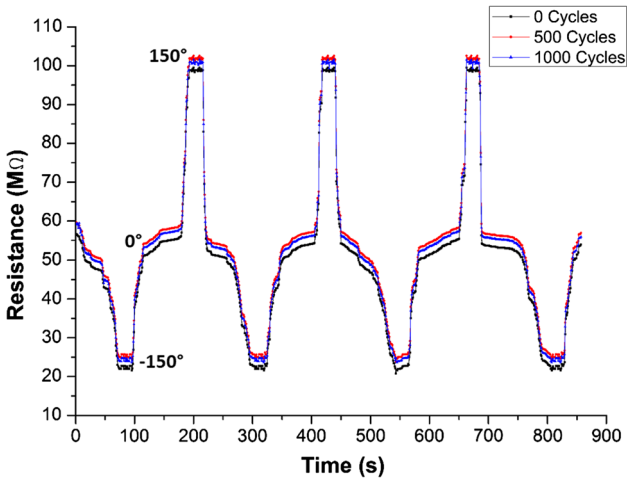

Fig. 10. Durability test of sensor with dimensions 3.5 cm × 1 cm after bending for up to 1000 cycles.

CONCLUSIONS

In conclusion, it can be stated that $ZnSnO_3$/PVDF composite thin films were fabricated and were employed successfully as a body motion flex sensor for measuring minor angular changes in posture. The piezo-electric β phase of PVDF polymer and the octahedral structure of $ZnSnO_3$ in composite form display excellent piezo-resistive properties and exhibit large changes in electrical resistance upon bending. The polymer also provides a binding matrix for the $ZnSnO_3$ cubes resulting in a robust piezo-resistive thin film. This feature is exploited to fabricate a highly stable motion sensor that can detect minor angular movements and can be used for applications like artificial skin. The maximum change recorded in resistive response of the sensors was ~20 MΩ to ~100 MΩ for bending angles of −150° to 150°. Durability tests for up to 1000 bending cycles show the excellent robustness, stability, and repeatability of the sensors.

ACKNOWLEDGEMENTS

We would like to acknowledge the financial support from the Global Leading Technology Program funded by the Ministry of Trade, Industry and Energy, Republic of Korea (10042477), the Ministry of Trade, Industry and Energy (MOTIE) and Korea Institute for Advancement of Technology (KIAT) through the Global collaborative R&D program, and the Ministry of Trade, industry & Energy (Ml, Korea) under Industrial Technology Innovation Program. No. 10052802, “Development of Roll-to-Roll continuous printing system for fine pattern/precision overlay patterning”.

CONFLICT OF INTEREST

The authors declare no conflict of interest.

ELECTRONIC SUPPLEMENTARY MATERIAL

The online version of this article (doi:10.1007/s11664-017-5370-7) contains supplementary material, which is available to authorized users.

REFERENCES

1. P. Kumar, J. Verma, and S. Prasad, *Int. J. Adv. Sci. Technol.* 43, 15 (2012).
2. N.H. Adnan, K. Wan, S. Ab, S. Khadijah, H. Desa, M. Azri, and A. Aziz, in *2nd Int. Malaysia-Irel. Jt. Symp. Eng.* (2012), p. 579.
3. S.K. Dixit and N.S. Shingi, *Int. J. Sci. Res. Publ.* 2, 2 (2012).
4. N.H. Adnan, K. Wan, A.B. Shahriman, M.H. Ali, M. Nasir Ayob, and A.A. Aziz, *Int. J. Mech. Mechatronics Eng.* 12, 41 (2012).

5. N. Tongrod, T. Kerdcharoen, N. Watthanawisuth, and A. Tuantranont, in *Int. Symp. Wearable Comput.* (IEEE, 2010), p. 1.
6. A. Raut, V. Singh, V. Rajput, and R. Mahale, *Int. J. Eng. Sci.* 1, 19 (2012).
7. D.V.K.B. Prakash and B. Gaikwad, *Int. J. Adv. Res. Comput. Sci. Softw. Eng.* 4, 1 (2012).
8. G. Saggio, *Sens. Actuators A Phys.* 205, 119 (2014).
9. S. Bakhshi and M.H. Mahoor, in *Proc. Int. Conf. Body Sens. Networks, BSN* (2011), p. 35.
10. G. Saggio, L. Bianchi, S. Castelli, M. Santucci, M. Fraziano, and A. Desideri, *Sensors* 14, 11672 (2014).
11. J.H. Pikul, P. Graf, S. Mishra, K. Barton, Y. Kim, J.A. Rogers, A. Alleyne, P.M. Ferreira, and W.P. King, *IEEE Sens. J.* 11, 2246 (2011).
12. G. Saggio, *Sens Actuators A Phys.* 185, 53 (2012).
13. J.E. Kesner, R.M. Gavalis, P.Y. Wong, and C.G.L. Cao, *Opt. Eng.* 50, 124402 (2011).
14. S. Endler, S. Ferwana, H. Rempp, C. Harendt, and J.N. Burghartz, *IEEE Electron Device Lett.* 33, 444 (2012).
15. J. Zhou, Y. Gu, P. Fei, W. Mai, Y. Gao, R. Yang, G. Bao, and Z.L. Wang, *Nano Lett.* 8, 3035 (2008).
16. N. Liu, G. Fang, W. Zeng, H. Long, L. Yuan, and X. Zhao, *J. Phys. Chem. C* 115, 570 (2011).
17. B. Radha, A.A. Sagade, and G.U. Kulkarni, *ACS Appl. Mater. Interfaces* 3, 2173 (2011).
18. L. Lin, S. Liu, Q. Zhang, X. Li, M. Ji, H. Deng, and Q. Fu, *ACS Appl. Mater. Interfaces* 5, 5815 (2013).
19. J.S. Lee, K. Shin, O.J. Cheong, J.H. Kim, and J. Jang, *Sci. Rep.* 5, 1 (2015).
20. J. Nunes-Pereira, V. Sencadas, V. Correia, V.F. Cardoso, W. Han, J.G. Rocha, and S. Lanceros-Méndez, *Compos. Part B Eng.* 72, 130 (2015).
21. Y. Qin, Q. Peng, Y. Ding, Z. Lin, C. Wang, Y. Li, F. Xu, J. Li, Y. Yuan, X. He, and Y. Li, *ACS Nano* 9, 8933 (2015).
22. M. Sajid, H.W. Dang, K.H. Na, and K.H. Choi, *Sens. Actuators A Phys.* 236, 73 (2015).
23. Y. Tang, Z. Zhao, H. Hu, Y. Liu, X. Wang, S. Zhou, and J. Qiu, *ACS Appl. Mater. Interfaces* 7, 27432 (2015).
24. M. Amjadi, M. Turan, C.P. Clementson, and M. Sitti, *ACS Appl. Mater. Interfaces* 8, 5618 (2016).
25. M. Borghetti, M. Serpelloni, E. Sardini, and S. Pandini, *Sens. Actuators A Phys.* 243, 71 (2016).
26. M.A. Darabi, A. Khosrozadeh, Q. Wang, and M. Xing, *ACS Appl. Mater. Interfaces* 7, 26195 (2015).
27. W. Obitayo and T. Liu, *J. Sens.* 2012, 652438 (2012).
28. C. Li, Y.-L. Cui, G.-L. Tian, Y. Shu, X.-F. Wang, H. Tian, Y. Yang, F. Wei, and T.-L. Ren, *Sci. Rep.* 5, 15554 (2015).
29. O. Kanoun, C. Müller, A. Benchirouf, A. Sanli, T.N. Dinh, A. Al-Hamry, L. Bu, C. Gerlach, and A. Bouhamed, *Sensors (Basel)* 14, 10042 (2014).
30. E. Roh, B.U. Hwang, D. Kim, B.Y. Kim, and N.E. Lee, *ACS Nano* 9, 6252 (2015).
31. S. Ryu, P. Lee, J.B. Chou, R. Xu, R. Zhao, A.J. Hart, and S. Kim, *ACS Nano* 9, 5929 (2015).
32. J.M. Wu, C.-Y. Chen, Y. Zhang, K.-H. Chen, Y. Yang, Y. Hu, J.-H. He, and Z.L. Wang, *ACS Nano* 6, 4369 (2012).
33. M. Kurata, X. Li, and K. Fujita, in *Proc. SPIE 8692, Sensors Smart Struct. Technol. Civil, Mech. Aerosp. Syst.* (2013), p. 1.
34. K.H. Choi, G.U. Siddiqui, B. Yang, and M. Mustafa, *J. Mater. Sci. Mater. Electron.* 26, 5690 (2015).